Modeling of Reduced Effective Secondary Electron Emission Yield from a Velvet Surface

Charles Swanson and Igor D. Kaganovich
Princeton Plasma Physics Laboratory, Princeton University, Princeton, New Jersey 08543

I. ABSTRACT

Complex structures on a material surface can significantly reduce total secondary electron emission from that surface. A velvet is a surface that consists of an array of vertically standing whiskers. The reduction occurs due to the capture of low-energy, true secondary electrons emitted at the bottom of the structure and on the sides of the velvet whiskers. We performed numerical simulations and developed an approximate analytical model that calculates the net secondary electron emission yield from a velvet surface as a function of the velvet whisker length and packing density, and the angle of incidence of primary electrons. We found that to suppress secondary electrons, the following condition on dimensionless parameters must be met: $(\pi/2)DA\tan\theta \gg 1$, where θ is the angle of incidence of the primary electron from the normal, D is the fraction of surface area taken up by the velvet whisker bases, and A is the aspect ratio, $A \equiv h/r$, the ratio of height to radius of the velvet whiskers. We find that velvets available today can reduce the secondary electron yield by 90% from the value of a flat surface. The values of optimal velvet whisker packing density that maximally suppresses secondary electron emission yield are determined as a function of velvet aspect ratio and electron angle of incidence.

PACS: 52.59.Bi, 52.59.Fn, 52.77.-j

II. INTRODUCTION

Secondary electron emission (SEE) from dielectric and metal surfaces under bombardment of incident electron flux is important for many applications where incident electron energy can reach tens or hundreds of electron volts. Under these conditions secondary electron emission yield can exceed unity and therefore strongly modify wall charging or cause multiplication of secondary electron populations. The multipactor effect causes accumulation of SEE population in RF amplifiers and limits the maximum electric field in these devices[1]. Clouds of secondary electrons have been also found to affect particle beam transport in accelerators. As a result, researchers at SLAC and CERN have studied effective ways to suppress Secondary Elecron Yield (SEY, γ) for example by cutting grooves into the accelerator walls[2–5]. SEE processes are also known to affect Hall thruster operation due to contribution to so-called near-wall conductivity or due to reducing wall potential and increasing plasma energy losses[6]. Wall conditions can also affect instabilities in plasmas and electron energy distribution functions[7,8]. Therefore, researchers investigate the possibility of using complex surface structures to minimize SEY for electric propulsion devices[9,10].

The surface geometry of a material can affect its SEY just as much as its chemical composition. Ruzic *et al.* are among those who experimentally found that surface treatments can affect SEY[11]. Alguilera *et al.* studied experimentally and theoretically velvet-covered surfaces for use in RF amplifiers to mitigate the effect of SEY[12]. Cimino *et al.* installed copper foam to produce dramatic SEY reductions[13]. Ye *et al.* investigated theoretically SEY reduction in walls with micro-pores, finding a strong dependence on geometry and predicting as much as 45% suppression of SEY[14]. Note that there is a significant difference in micro-pores configuration as opposed to velvet; in micro-pores configuration electrons cannot penetrate arbitrary far along perpendicular distances into the pore array, unlike in velvet. As an important consequence, we show that velvets can give much higher reduction in SEY as compared to micro-pores configuration.

In this paper we study reduction in SEY by velvet surfaces both analytically and numerically. A velvet surface is a flat substrate onto which long, vertical whiskers are grown. The reduction of SEY comes from the fact that low-energy true secondary electrons produced deep inside the velvet have a large probability of hitting a whisker and getting absorbed by the surface before exiting the velvet, therefore not contributing to net SEY from the surface.

Baglin *et al.* experimentally characterized the secondary electron emission of dendritic copper, which has features very much like the whiskers of velvet[15]. They found reductions in the SEY of $> 65\%$. While we examine the effect of geometry for graphitic material, our results do produce a similar reduction for the same velvet parameters as in Ref.[15].

More recently, Huerta and Wirz have performed Monte Carlo modeling to characterize the SEY from copper velvet and fuzz surfaces[16]. They, like we do, find reductions of SEY which have strong dependencies on the dimensionless packing densities and aspect ratios, though they do not explore this dependence analytically and do not cover the dynamic range of aspect ratios that we do.

We have developed an analytical model of SEE of a velvet surface and determined an analytical expression for the SEY, γ, of such a surface as a function of the velvet parameters. We also simulated the SEE process numerically and benchmarked the analytical model against

the simulation results. Based on the analytical model, we calculated approximate values of the optimal packing density and aspect ratio of the whiskers to achieve minimum SEY as a function of a primary angle of incidence.

Carbon velvet surfaces as available today have characteristic diameters of a few microns, and characteristic lengths of a few millimeters[9]. The following analysis assumes that secondary electron emission takes place only at a material surface, with no volume effects. Because of this, our analysis holds for whisker radius r larger than the scale of primary electron penetration in carbon, tens of nanometers,

$$r \gg 10nm. \qquad (1)$$

Our analysis assumes the whiskers are grown onto a flat substrate, and that electrons come from far away. Because of this, both the inter-whisker spacing, s, and the whisker length h should be much smaller than the characteristic scale length of the device, L:

$$s \ll L, \qquad (2)$$

$$h \ll L. \qquad (3)$$

Furthermore, our analysis assumes that velvet fibers are perfectly normally oriented. In actuality, velvet fibers are observed to lie at angles to the normal, and even to curve and change their angles, to "flop" over near their tops[9]. This effect is not considered by our model.

III. DESCRIPTION OF NUMERICAL SIMULATIONS OF SEE PROCESS IN VELVET SURFACES

In principle, it is possible to simulate electron propagation in the vacuum and inside the material, see e.g. Ref.[17]. However, the full simulation is beyond necessity for our problem. Instead, we assume the SEY of a flat surface to be known and only propagate electrons in vacuum. We also assume that plasma does not penetrate into the whisker region because the Debye radius is large compared with the distance between whiskers. The opposite limit when sheath forms near two walls/surfaces and strongly affect combined SEY of two surfaces is studied in Refs.[19,20]. When an electron impacts the surface, SEE is produced according to known SEY of that surface and incident angle. For a velvet surface, we have to take into account contributions from the secondary electrons emitted by the whisker side, top, and bottom surfaces. The electron velocity distribution function (EVDF) is described by velocity, v, spherical angles, θ, ϕ, and electron position x, y, z as shown in Fig. 1. Geometrical quantities of the whiskers are the whisker radius, r, whisker height h, and spacing between whiskers, $2s$. We introduce the notation of aspect ratio,

$$A = h/r$$

and packing density,

$$D = \frac{\pi r^2}{(2s)^2},$$

which is the proportion of surface area of the bottom taken up by the base of the whiskers, see Fig. 1. In the numerical simulations, we studied a regular lattice of whiskers and therefore used only one segment around one whisker with a periodic boundary condition; particles exiting the simulation domain were re-introduced into the opposing side with identical velocity, as if the whiskers are arranged on a regular square grid.

We numerically simulated the emission of secondary electrons by using the Monte Carlo method, initializing many particles and allowing them to follow ballistic, straight-line trajectories until they interact with surface geometry. A flowchart of the algorithm is in Fig. 2. In the results presented here, we used 10^5 particles. Each particle object keeps track of seven quantities: its three spatial positions x, y, z, its energy, E, and velocity angles θ, ϕ, and its "weight," meaning how many particles it stands for. All weights start at a value of 1. Weights are changed upon interaction with a surface.

An alternate approach would be to start with fewer particles and have them stand for a fixed number of particles, all with weight 1. When SEY occurs, in this approach one would instantiate more particles until one tallies 10^5. Starting with 10^5 and instead changing the weights upon SEY produces identical counting statistics, with error associated with counting statistics being $N^{-1/2} = 0.3\%$.

The surface geometry and initial distribution of incident particles are the simulation's main input parameters. The velvet surface geometry is represented as cylindrical whiskers implemented as an isosurface of a function of space, as collisions with an isosurface are trivially detectable by a particle object which stores its spatial location. We used an isosurface function for which $F_{iso} = 0$ defines a flat-topped cylinder with height h and radius r with a flat floor at $z = 0$, with $F_{iso} < 0$ being inside the cylinder and $F_{iso} > 0$ being outside the surface.

At every time step, we checked to see whether particles had passed into the surface. If they had, their local normal angle was determined relative to the gradient of F_{iso}, and the SEY of their energy and local normal angle was computed. Their weight was multiplied by the SEY.

Emitted particles were given a new velocity angle. Secondary electrons were emitted with probability linearly weighted by the cosine of the normal angle[24]. Thus

$$P(\Omega)d\Omega = 2\cos\vartheta\, d\cos\vartheta \frac{d\phi}{2\pi} \qquad (4)$$

where ϑ is computed relative to the local normal, $\vec{\nabla}F_{iso}$. Specifically in the code, $\cos\vartheta = R^{1/2}$, where R is a uniform random variable from 0 to 1. The azimuthal angle
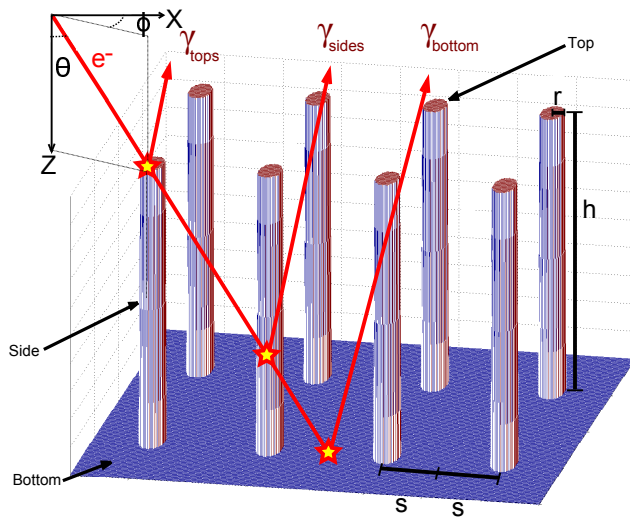
FIG. 1. Schematics of the velvet surface: the whisker geometrical quantities radius, r, height, h, and spacing, $2s$. Also shown are electron velocity polar angle θ, and velocity azimuthal angle, ϕ. Numerical calculations include three contributions to secondary electron emission from velvet: electrons emitted by the side, top, and bottom surface of the whiskers.

in the local normal frame was uniformly distributed from 0 to 2π.

It is interesting to note the differences between flux and velocity distribution function, and how they characterize the number of electrons with a certain velocity. As flux is total number of particles that pass through a differential cross sectional area oriented along some normal $\hat{n}$, flux is

$$\Gamma = \int d^3 v \vec{v} \cdot \hat{n} f(\vec{v}) \qquad (5)$$

for distribution function $f(\vec{v})$. That is, flux counts particles *passing through* a surface while distribution function counts particles *within* a volume. Thus, though probability and flux are weighted by $\cos\vartheta$, this is the condition that the distribution function $f(\vec{v})$ is isotropic in angle.

The SEY of the incident electron is computed using several different *a priori*, empirical, and semi-empirical expressions. We used one of the latter, that of Scholtz,[21]

$$\gamma\left(E_p, \theta\right) = \gamma_{max}(\theta) \times \exp\left[-\left(\frac{\ln[E_p/E_{max}(\theta)]}{\sqrt{2}\sigma}\right)^2\right]. \qquad (6)$$

where the parameters $E_{max}, \gamma_{max}, \sigma$ are free parameters of the Scholtz model. Angular dependence is taken from Vaughan[22],

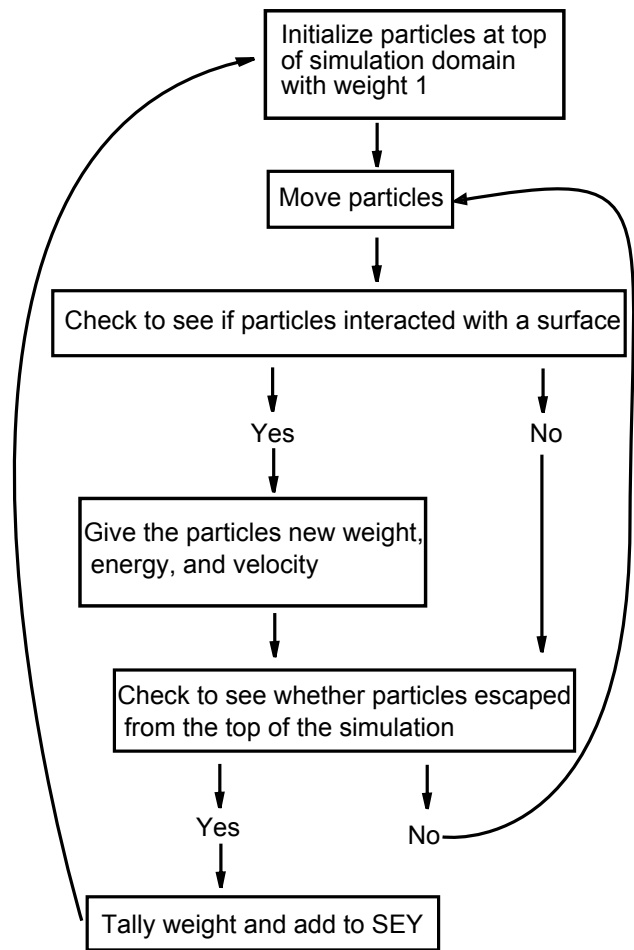$$\gamma_{max}(\theta) = \gamma_{max_0}\left(1 + \frac{k_s\theta^2}{2\pi}\right)$$

FIG. 2. Flowchart of the Monte Carlo simulation algorithm.

$$E_{max}(\theta) = E_{max_0}\left(1 + \frac{k_s\theta^2}{\pi}\right).$$

The specific constants in the Scholtz model were taken from the graphite experimental data given in Patino *et al.*[23], $\gamma_{max_0} = 1.2, E_{max_0} = 325eV, \sigma = 1.6, k_s = 1$. The semi-empirical model of Scholtz was chosen because it agrees well with Patino *et al.* experimental data for graphite.

Emitted electrons have three energy-groups. True secondary electrons were given a low few eV temperature. Elastically scattered electrons were given the same energy as the primary electrons. Rediffused electrons were given energy uniformly distributed between zero and the primary electron energy. True secondary electrons, elastically scattered electrons, and inelastically scattered (rediffused) electrons were simulated with the energy-dependent probabilities of emission reported in Ref.[23]. In accordance with that experiment, we used following empirical formula for fraction of elastically scattered electrons, f_{el}:

$$f_{el}(E_p) = \exp\{1.59 + 3.75\ln(E_p) - 1.37\left[\ln(E_p)\right]^2$$
$$+0.12\left[\ln(E_p)\right]^3\}.$$

<div align="right">(7)</div>

for $E_p = 6 - 390eV$, and $f_{el}(E_p) = 100\%$ for $E_p < 6eV$, for $E_p > 390eV$, $f_{el}(E_p) = 2\%$. The fraction of inelastic electrons was assumed to be equal to 7%, where permitting by $f_{el} < 93\%$. The values of SEY calculated using this formula will prove to be sensitive to the fraction of elastically scattered electrons, as these electrons are not absorbed by surfaces, and can still contribute their full number to the SEY.

The remaining, true secondary electrons were given a Maxwellian EVDF with temperature $T_{true} = 5.4eV$[23].

Simulations presented here were performed for electron incident energy of 200eV. The sensitivity of the resulting SEY to this primary energy is not large; simulations performed at 400eV had the effect of increasing the tertiary electrons created by elastically scattered secondary electrons, but these only account for 2% of secondary electrons at this energy.

We found that adding velvet to a surface can significantly decrease the net SEY of velvet surface as much as 90% from the case of normal incidence on a flat surface. The reduction in SEY depends strongly on the velvet parameters: packing density, D, and aspect ratio, A. To achieve 90% reduction in SEY, $A = 100 - 1000$, and $D = 4\%$ are required as evident in Fig. 3. Such velvets with aspect ratio $A = 1000$ and packing density $D = 4\%$ can be currently grown in the laboratory[9]. The net SEY of velvet is a strong function of the incident angle θ. However, for all angles the net SEY is always below 50% of the SEY of the flat surface without velvet for high aspect ratio A, see Fig. 3.

To understand the dependencies of the SEY on the velvet parameters shown in Fig. 3, an analytical model is developed and discussed in the next section. It resolves the apparent contradiction of why the trend of SEY with θ reverses between the values of $A = 10$ and $A = 100$. For the first of these cases, the majority of the SEY is contributed by the bottom substrate. For the second, the majority of the SEY is contributed by the sides of the cylinders. This is described in the following analysis by the value of the dimensionless parameter $u\tan\theta$, which crosses unity between these two cases. The significance of this difference is explored fully in Section V.

IV. ANALYTIC EXPRESSION FOR THE NET SEY OF THE VELVET SURFACE

In the simulations we assumed that whiskers form a rectangular lattice. This assumption helps computational tractability by introducing periodic pattern and reducing simulation volume to one periodicity element. For the analytic calculation it is much easier to assume
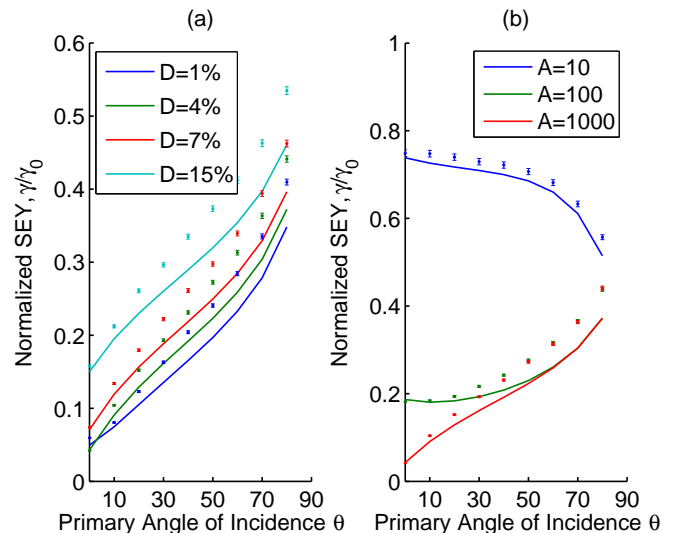

FIG. 3. SEY reduction from the case of normal incidence on a flat surface. SEY reduction is given as a function of incident angle, θ, for different values of whisker aspect ratio A, and packing density D. Figure (a) shows SEY for 4 different D values and the same $A = 1000$. Figure (b) shows SEY for 3 different values of A and the same $D = 4\%$. Solid lines show the result of an analytic approximation. Points with error bars are the result of these Monte Carlo simulations. The simulation results are compared to the analytic approximation given in section IV, Eq.23.

instead that whiskers are positioned along the surface randomly. We show that substituting regular lattice whiskers instead with a random distribution of whiskers having the same average packing density does not introduce significant change in SEY. The probability for a secondary electron to intersect a whisker is similar for regular and random pattern of whiskers. Qualitative agreement between mean-free-paths given by the rectangular lattice and random lattice assumptions is shown in Fig. 4. In the random position case, this probability of not being intersecting with a whisker can be described by exponential dependence with the distance in the $x-y$ plane perpendicular to the whiskers' axis, $l_\perp$. This probability is given by

$$P_{free}(l_\perp) = e^{-l_\perp/\lambda_\perp}.$$

<div align="right">(8)</div>

The mean-free-path is $\lambda_\perp$

$$\lambda_\perp = \frac{1}{2rn}.$$

<div align="right">(9)</div>

where $n = 1/(2s)^2$ is the surface density of whiskers. This mean-free-path is determined from analogy to classical hard-sphere scattering in 3D. The cross section length that a cylinder presents is twice its radius, and the "scattering density" is simply the surface area density of whiskers, n.
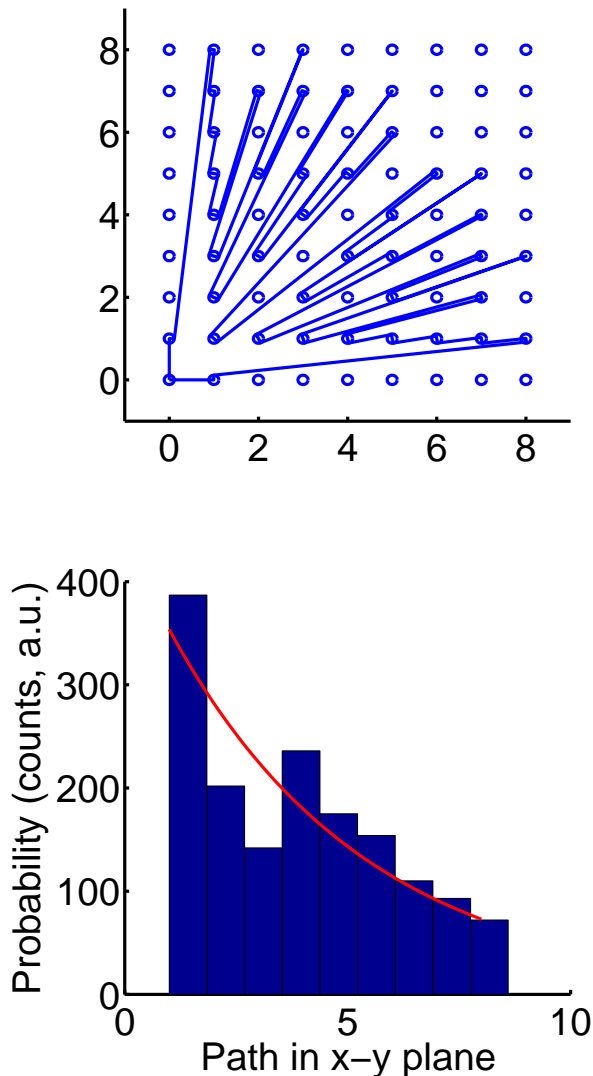
clusion would add complexity to the formulae derived. The sequential secondary electrons can be added to the treatment in the future. The error associated with this truncation can be as high as 10%, as per Equation 7

The secondary electron emission can occur on one of three surfaces: on the top of the whisker, on the side surface, and on the bottom surface, as shown in Fig. 1. Hence the net γ_{eff} consists of three contributions:

$$\gamma_{eff} = \gamma_{top} + \gamma_{bottom} + \gamma_{sides}. \tag{10}$$

The top contribution is simply proportional to the ratio of surface of the top whiskers to the rest of the surface. Consider a plane just below the whisker tops. The electrons have a uniform probability of hitting any area of that plane. Those electrons which hit the cylinder tops, whose area is D of the total, will cause SEE from the tops. Those electrons which hit elsewhere on the notional plane will penetrate into the whisker layer and hit either the sides or the bottom surface. Therefore,

$$\gamma_{top} = \gamma(\theta)D. \tag{11}$$

The sides and bottom contributions require calculation of probability to hit a side surface of the whisker. As discussed above, the probability of intersection of a side surface of the whisker can be assumed to be constant per unit distance traveled parallel to the surface (or perpendicular to the axis of the whisker), which is $l_\perp = z \tan\theta$, where z is the distance traveled along the z-axis in the velvet layer and θ is again the angle between the z-axis and electron velocity. Thus the probability for one electron to *not intersect* a side surface of the whisker is given by

$$P_{free}(z,\theta) = e^{-2rnz\tan\theta}. \tag{12}$$

This is the cumulative probability to not have hit by depth z. The differential probability to *intersect* a whisker side at z is given by $-\partial P_{free}(z,\theta)/\partial z$. The product of this and the probability to not hit the tops $(1-D)$ is the probability that one electron, coming in from above the whisker tops at angle θ, will hit a whisker at a height z

$$P_{hitside}(z) = -(1-D)\frac{\partial}{\partial z}P_{free}(z,\theta). \tag{13}$$

To simulate how many secondaries emitted on a side surface can reach back to free space, we need to calculate probability of emission as a function of the velocity direction. In order to describe emitted electron velocity direction we use the coordinate system that is placed at the whisker side as shown in Fig. 5. In polar angles around z-axis, we introduce angle, θ_2 between z-axis and emitted electron velocity and azimuthal angle, ϕ. We
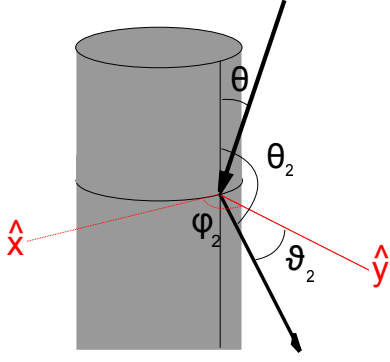

FIG. 4. Top: Schematics showing the top view of the velvet with regular pattern of whiskers for $D = 4\%$. Blue lines show the maximum extent of trajectories emitted at 1500 values of ϕ, evenly spaced between 0 and $\pi/2$, originating at point $0, 0$. Bottom: Probability histogram of mean-free-path for $D = 4\%$ for the rectangular case. 1500 trajectories, evenly spaced in ϕ, were calculated. The red curve is $\exp(-l_\perp/\lambda_\perp)$, corresponding to random configuration of whisker positions.

From Fig. 4 it is evident that for a rectangular lattice of whiskers and a random configuration with the same packing density, the mean-free-path is similar.

Our analytic model takes only one generation of true secondary electrons into consideration. We neglect sequential secondary electrons caused by the first generation of secondary electrons. Neglecting their contribution is the largest source of error of the analytic, but their in-

FIG. 5. Angle θ is the polar angle of the primary electron. Angle θ_2 is the polar angle of the secondary electron. Angle ϑ_2 is the local normal angle of the secondary electron. ϕ is the primary azimuthal angle. ϕ_2 is the secondary azimuthal angle.
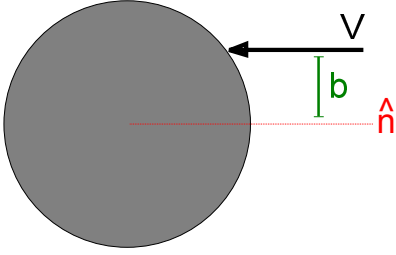

FIG. 6. Definition of the impact parameter, b. Cylinder is seen from tops, view aligned along z axis.

also use polar angle ϑ_2 between local normal and emitted electron velocity and in this same frame, a local normal azimuthal angle ϕ_2. If we assume that the normal to the whisker surface coincides with the y-axis, the ϑ_2 angle between between y-axis and emitted electron velocity is given in terms of polar angles θ_2 and ϕ according to

$$\cos \vartheta_2 = \sin \theta_2 \sin \phi. \qquad (14)$$

The probability distribution emitted over solid angle, $\Omega_2(\theta_2, \phi_2)$ is

$$P(\Omega_2) = 2 \cos \vartheta_2 \Theta(\cos \vartheta_2). \qquad (15)$$

Here Θ is the Heviside function and we accounted for the fact that emission flux is proportional to cosine of angle between of emitted electron velocity direction and normal to the surface, Eq.(4). Averaging over azimuthal angle ϕ_2 we obtain probability of electron emission with angle θ_2

$$P(\theta_2) \equiv \int_0^{2\pi} \frac{d\phi}{2\pi} \sin \theta_2 P(\theta_2, \phi_2) = \frac{2}{\pi} \sin^2 \theta_2. \qquad (16)$$

Therefore the SEY of the sides of the velvet whiskers is

$$\gamma_{side}(\theta) = \frac{2}{\pi}(1 - D) \langle \gamma(\theta) \rangle_b \int_0^{\pi/2} d\theta_2 \sin^2 \theta_2$$
$$\times \int_0^h dz P_{free}(z, \theta_2) \frac{\partial}{\partial z} P_{free}(z, \theta). \qquad (17)$$

$\langle \gamma(\theta) \rangle_b$ is necessary to compute because the local polar angle ϑ depends not only on the absolute polar angle θ but also the impact parameter at which the electron strikes (see Fig. 6); that is an electron which hits a fiber dead-on will have $\vartheta = \pi/2 - \theta$, but an electron which hits at a glancing angle will have $\vartheta = \pi/2$. Averaging $\gamma(\vartheta)$ over this impact parameter b gives

$$\langle \gamma(\theta) \rangle_b = \int_0^1 db \gamma(\cos^{-1}(\sin \theta \sqrt{1 - b^2})). \qquad (18)$$

Using Scholtz's and Vaughan's expressions for SEY, this averaged SEY, $\langle \gamma(\theta) \rangle_b$, was never more than about 30% higher than the flat value, $\gamma(\theta)$. Substituting equation 12 into equation 17 and introducing notation $t = \tan \theta_2$, equation 17 becomes

$$\gamma_{side}(\theta) = \frac{2}{\pi}(1 - D) \langle \gamma(\theta) \rangle_b \tan \theta$$
$$\times \int_0^\infty dt \frac{t^2}{(1+t^2)^2} \frac{1 - e^{-2rnh(t+\tan\theta)}}{t + \tan \theta} \qquad (19)$$

Similarly for the contribution from the bottom surface,

$$\gamma_{bottom}(\theta) = 2(1 - D)\gamma(\theta) \int_0^{\pi/2} d\theta_2$$
$$\times \sin \theta_2 \cos \theta_2 P_{free}(h, \theta_2) P_{free}(h, \theta), \qquad (20)$$

or in the same notation as equation 19,

$$\gamma_{bottom}(\theta) = 2(1 - D)\gamma(\theta) \int_0^\infty dt \frac{t e^{-2rnh(t+\tan\theta)}}{(1+t^2)^2}. \qquad (21)$$

It is apparent from equations 19 and 21 that the dimensionless parameter

$$u = 2rnh = \frac{2rh}{(2s)^2} = \frac{2}{\pi}DA \qquad (22)$$

is the relevant parameter to characterize a SEY from the velvet surface. The total SEY can be written

$$\gamma_{eff}(\theta) = \gamma(\theta)\left[D + (1 - D)f(u, \theta)\right], \qquad (23)$$

where

$$f(u, \theta) = 2 \int_0^\infty dt \frac{t e^{-u(t+\tan\theta)}}{(1+t^2)^2}$$
$$+ \frac{\langle \gamma(\theta) \rangle_b}{\gamma(\theta)} \tan \theta \frac{2}{\pi} \int_0^\infty dt \frac{t^2}{(1+t^2)^2} \frac{1 - e^{-u(t+\tan\theta)}}{t + \tan \theta}. \qquad (24)$$

From Fig. 3 it is evident that the predictions of the analytical model of velvet SEY agrees well with the numerical simulation results. The differences are due to approximations: First, only one generation of electrons is considered analytically. Second, the geometry simulated is a rectangular lattice rather than the continuous distribution of scattering centers assumed by the analytical model. The depicted simulation error derives from counting statistics, with $\delta\gamma \propto \sqrt{N}, N = 10^5$. Therefore stochastic counting error $< 1\%$.

V. DEPENDENCE OF THE NET SEY ON WHISKERS PROPERTIES

Having the analytic expression for the net secondary electron emission yield (SEY, γ_{eff}) given by equation 23 allows for analysis of optimum whisker properties for reduction of γ_{eff}. Firstly, analysis shows that $f(u, \theta)$ is a monotonically decreasing function of the dimensionless parameter u, and therefore is a monotonically decreasing function of whisker height, see equation 22 . This is expected; because as whisker height increases, electrons instead of hitting the bottom surface would penetrate deeper into the whisker region further from the top of whisker surface. Any secondary electrons produced by these electrons will have a longer distance to traverse and large probability to hit whiskers again and therefore net SEY is reduced.

The relative contributions from bottom and sides of whiskers is determined by value of parameter $u \tan\theta$, as evident by comparing terms in equation 24. In the limit of high $u \tan\theta$

$$u \tan\theta \gg 1$$

the contribution of the SEY from the bottom surface into the net SEY is negligible, because electrons hit a whisker near the tops with higher probability. In the opposite limit

$$u \tan\theta \ll 1$$

the SEY from the bottom surface is significant, because electrons are more likely to hit the bottom surface at these conditions and these secondary electrons are more likely to escape. Moreover in this limit contribution from the bottom surface is reduced for a more shallow angle, θ; whereas contribution from side surfaces is increased for a more shallow angle, θ. This is demonstrated in Fig. 7.

In Fig. 3, the only case in which $u < 1$ corresponds to $A = 10, D = 4\%$, in which $u \approx 0.25$. As explained above the main contribution to the SEY in this case is from the bottom surface and the net SEY is a decreasing function of the incident angle.

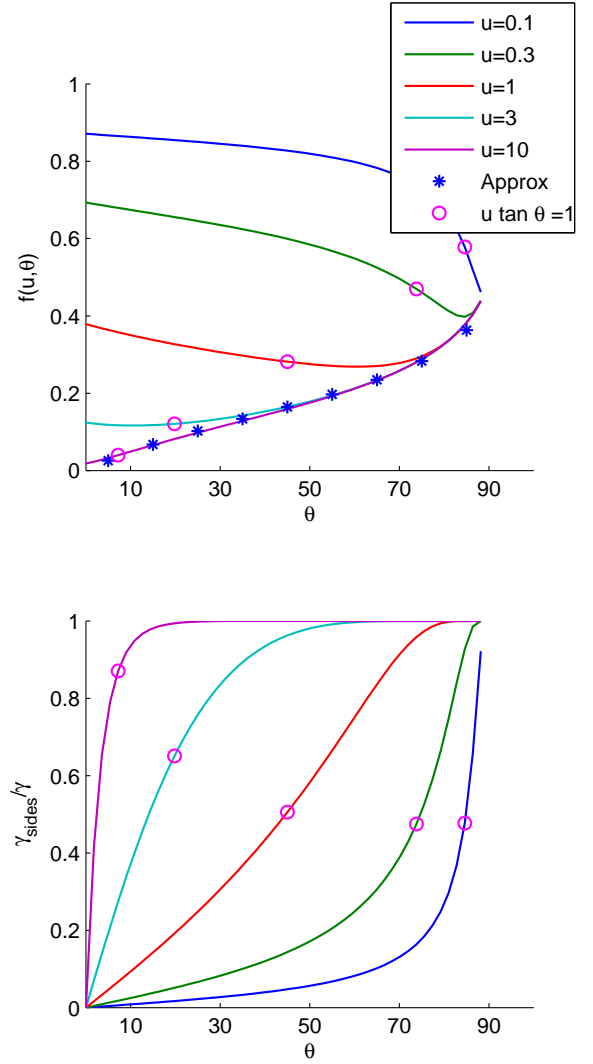In the opposite limit $u \tan\theta >> 1$, the functional form of the SEY becomes

FIG. 7. Top: $f(u,\theta)$ vs θ for several u (curves) that determines the net SEY in equation $\gamma_{eff} = \gamma_{flat}\{D + (1 - D)f(u,\theta)\}$, including the approximation given by equation 26 (blue symbols). Bottom: Relative contribution to the SEY of the sides of the whiskers. Pointed out in both are the points at which the quantity $u \tan\theta$ crosses unity.

$$\lim_{u\tan\theta\to\infty} \gamma_{eff} = \gamma(\theta)D + \frac{2}{\pi} \langle \gamma(\theta)\rangle_b (1 - D)$$
$$\times \int_0^\infty dt \frac{t^2 \tan\theta}{(1 + t^2)^2(\tan\theta + t)}, \tag{25}$$

which is the contribution from whisker tops and sides only (no contribution from bottom). As evident from equation 25 increasing whisker length (h) above $u \tan\theta = 2rnh \tan\theta > 1$ will not affect the SEY.

For the expression given by equation 25 we have developed an approximate expression in the form
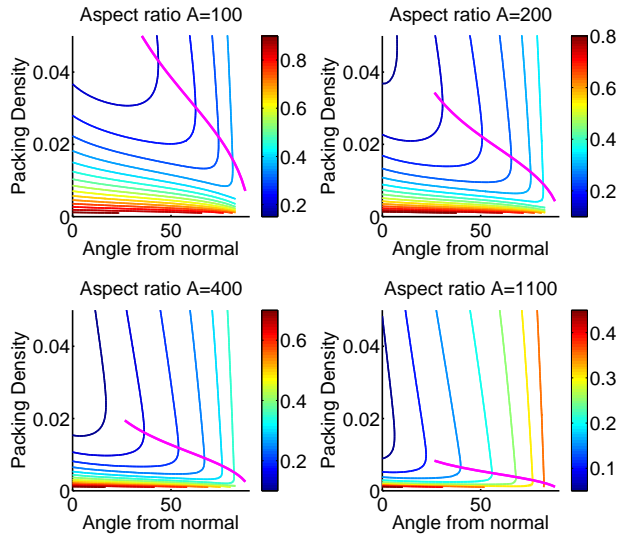
FIG. 8. Reduction of Secondary Electron Yield (ratio of the net SEY to that of a flat surface) as function of whiskers packing density and incident angle. Magenta line shows optimal value of packing density $D(\theta)$ corresponding to the minimum net SEY.

$$\lim_{u\tan\theta\to\infty} \gamma_{eff} \approx \gamma(\theta)D + \frac{1}{2}\langle\gamma(\theta)\rangle_b (1-D)$$
$$\times \left[1 - \frac{1}{(1.39\tan\theta+1)^{0.45}}\right], \qquad (26)$$

with average deviation of 0.5% from the exact result. This function is depicted in Fig. 7 (blue symbols).

1. Optimization of velvet parameters for SEY reduction

In this section we investigate the velvet parameters that give SEY the most reduction. Figure 8 shows SEY as a function of packing density and incidence angle for given aspect ratio of whiskers.

From Fig. 8 it is evident that there is an optimal packing density that yields the minimum net SEY for a set aspect ratio A. Indeed at large values of $D \to 1$ the contribution of SEY from the whisker tops dominates the net SEY the net SEY increases with the packing density. At small values of $D \to 0$ and large values of A so that $\frac{2}{\pi}DA\tan\theta \gg 1$ the contribution of sides dominates and

$$\lim_{\substack{\frac{2}{\pi}DA\tan\theta\gg1 \\ D\to0}} \gamma_{eff} \to \frac{1}{2}\langle\gamma(\theta)\rangle_b \left[1 - \frac{1}{(1.39\tan\theta+1)^{0.45}}\right]$$
$$(27)$$

and for very small values of $D \to 0$ such that $\frac{2}{\pi}DA\tan\theta \ll 1$ contribution of the bottom of whiskers

dominates and taking appropriate limit in equation 23 gives

$$\lim_{\substack{\frac{2}{\pi}DA\tan\theta\ll1 \\ D\to0}} \gamma_{eff} \to \gamma(\theta). \qquad (28)$$

That is at very low values of D there are simply not enough whiskers for any significant number of electrons to intersect them when traversing the velvet.

Therefore the optimum value of whisker parameters corresponding to minimum SEY is approximately given by the condition

$$\frac{2}{\pi}DA\tan\theta \sim 1. \qquad (29)$$

Investigation of Fig. 8 allowed us to derive the location of the optimal D to minimize net SEY, γ_{eff} for given values of A, θ. This optimal $D_{optimal}$ is approximately given by

$$D_{optimal}(\theta) \approx 0.97\frac{\ln(A)}{A(\tan\theta)^{0.47}} - \frac{0.26}{A}. \qquad (30)$$

Equation 30 gives agreement with 12% average error for the position of the optimal D as shown in Fig. 8.

VI. CONCLUSIONS

We have investigated numerically and analytically the effect of velvet surfaces on secondary electron emission (SEE) and concluded that the net secondary electron yield (SEY) can be reduced dramatically by application of velvet to the surface. Geometrical quantities of the whiskers are the whisker radius, r, whisker height, h, and spacing between whiskers, $2s$. The beneficial velvet configuration for the net SEY reduction consists of high aspect ratio long whiskers,

$$A \equiv h/r, \qquad (31)$$

rarely placed on the surface with low packing density

$$D \equiv \pi r^2/(2s)^2 \to 0, \qquad (32)$$

such that

$$\frac{2}{\pi}DA\tan\theta \gg 1.$$

In this case incident electrons do not reach the bottom of the velvet and large fraction of the secondary electrons emitted from the side do not exit the velvet, because they are intersected by whiskers again. The approximate net SEY is given in this case by

$$\lim_{\substack{\frac{2}{\pi}DA\tan\theta\gg1 \\ D\to0}} \gamma_{eff} \to \frac{1}{2}\langle\gamma(\theta)\rangle_b \left[1 - \frac{1}{(1.39\tan\theta+1)^{0.45}}\right]$$
$$(33)$$

where

$$\langle \gamma(\theta) \rangle_b = \int_0^1 db \gamma(\cos^{-1}(\sin\theta\sqrt{1-b^2})). \qquad (34)$$

From equation 33 it is evident that it is possible to decrease SEY by more than 50% for shallow incidence ($\tan\theta \sim 1$) and more than 90% for normal incidence ($\theta \ll 0.7$) compared to the case of normal incidence on a flat surface.

The optimal packing density for reducing SEY depends on the angle of incidence of the primary electrons and is approximately given by

$$D_{optimal}(\theta) \approx 0.97 \frac{\ln(A)}{A(\tan\theta)^{0.47}} - \frac{0.26}{A}. \qquad (35)$$

Equation 35 gives agreement with 12% average error for the position of the optimal D as shown in Fig. 8.

In summary, using plausible values for parameters of lab-grown velvets ($A > 100$), we find that velvet surfaces are a promising candidate for reducing SEY by more than 50% for shallow incidence ($\tan\theta \sim 1$) and more than 90% for normal incidence ($\theta \ll 0.7$) compared to the case of normal incidence on a flat surface. The closer to the normal is the angle of incidence, the more a long, non-dense velvet can suppress the SEY. Interestingly, if it is known that the incident electron flux has a *narrow* distribution of incident angles, one could use a velvet with whiskers oriented not normally but along that direction; such velvet is the most efficient way to minimize SEY.

A. Acknowledgment

[1] J. R. M. Vaughan, *Multipactor*, IEEE Trans. Electron Devices **35**, 1172-1180 (1988).

[2] G. Stupakov and M. Pivi, *Suppression of the Effective Secondary Emission Yield for a Grooved Metal Surface*, Proc. 31st ICFA Advanced Beam Dynamics Workshop on Electon-Cloud Effects, Napa, CA, USA, April 19-23, 2004.

[3] L. Wang *et al.*, *Suppression of Secondary Electron Emission using Triangular Grooved Surface in the ILC Dipole and Wiggler Magnets*, Proc. of Particle Accelerator Conference (PAC 2007), Albuquerque, NM, USA, June 25-29, 2007.

[4] M. T. F. Pivi *et al.*, "Sharp Reduction of the Secondary Electron Emission Yield from Grooved Surfaces," J. Appl. Phys. **104**, 104904 (2008)

[5] Y. Suetsugu *et al.*, *Experimental Studies on Grooved Surfaces to Suppress Secondary Electron Emission*, Proc. IPAC'10, Kyoto, Japan, 2021-2023 (2010).

[6] Y. Raitses, *et al.*, "Effect of Secondary Electron Emission on Electron Cross-Filed Current in $E \times B$ Discharges," IEEE Trans. on Plasma Scie. **39**, 995 (2011).

[7] D. Sydorenko, I. Kaganovich, Y. Raitses, and A. Smolyakov, "Breakdown of a Space Charge Limited Regime of a Sheath in a Weakly Collisional Plasma Bounded by Walls with Secondary Electron Emission", Phys. Rev. Lett. **103**, 145004 (2009).

[8] A. I. Smolyakov, W. Frias, I. D. Kaganovich, Y. Raitses, *Sheath-Induced Instabilities in Plasmas with ExB Drift*, Phys. Rev. Lett. **111**, 115002 (2013).

[9] Y. Raitses, *et al.*, "Operation of a segmented Hall thruster with low-sputtering carbon-velvet electrodes." J. Appl. Phys. **99,** 36103 (2006).

[10] Y. Raitses, I. D. Kaganovich and A. V. Sumant, *Electron Emission from Nano- and Micro-Engineered Materials Relevant to Electric Propulsion*, IEPC-2013-390, the 33rd International Electric Propulsion Conference, The George Washington University, Washington, D.C., USA, October 6 - 10, 2013.

[11] D. Ruzic, R. Moore, D. Manos, and S. Cohen *Secondary electron yields of carbon-coated and polished stainless steel*, J. Vac. Sci. Technol. **20,** 1313 (1982).

[12] L. Aguilera *et al.* "CuO Nanowires for Inhibiting Secondary Electron Emission," J. Phys. D: Appl. Phys. **46**, 165104 (2013).

[13] R. Cimino *et al.*, "Search for New e-cloud Mitigator Materials for High Intensity Particle Accelerators," Proc. of IPAC2014, Dresden, Germany 2332-2334 (2014).

[14] M. Ye *et al.*, "Suppression of Secondary Electron Yield by Micro-Porous Array Structure," J. Appl. Phys. **113**, 074904 (2013).

[15] V. Baglin, J. Bojko, O. Grabner, B. Henrist, N. Hilleret, C. Scheuerlein, M. Taborelli, *The secondary electron yield of technical materials and its variation with surface treatments*, Proceedings of EPAC 2000, 26-30 June 2000, Austria Center, Vienna, pp. 217-221.

[16] Huerta, Cesar E., and Richard E. Wirz. *Surface Geometry Effects on Secondary Electron Emission Via Monte Carlo Modeling.* In 52nd AIAA/SAE/ASEE Joint Propulsion Conference. American Institute of Aeronautics and Astronautics, July 25 2016. http://arc.aiaa.org/doi/abs/10.2514/6.2016-4840.

[17] Z. Insepov, V. Ivanov, H. Frisch, *Comparison of candidate secondary electron emission materials*, Nuclear Instruments and Methods in Physics Research B: Beam Interactions with Materials and Atoms **268**, 3315-3320 (2010).

[18] Z. J. Ding, X. D. Tang, and R. Shimizu, "Monte Carlo study of secondary electron emission", Journal of Applied Physics 89, 718 (2001);

[19] Hongyue Wang, Michael D. Campanell, Igor D. Kaganovich, Guobiao Cai, "Effect of asymmetric secondary emission in bounded low-collisional E×B plasma on sheath and plasma properties", Journal of Physics D: Applied Physics, **47**, 405204 (2014).

[20] M D Campanell, H Wang, I D Kaganovich and A V Khrabrov, "Self-amplification of electrons emitted from surfaces in plasmas with $E \times B$ fields", Plasma Sources Science and Technology 24, 34010 (2015).

[21] J. Scholtz *et al.*, "Secondary Electron Emission Properties," Phillips J. Res. **50**, 375 (1996).

[22] J. Vaughan, "A New Formula for Secondary Emission Yield", IEEE Trans. on Electron Devices **36,** 9 (1989).

[23] M. Patino, Y. Raitses, B. Koel and R. Wirz, *Application of Auger Spectroscopy for Measurement of Secondary Electron Emission from Conducting Material for Electric Propulsion Devices*, IEPC-2013-320, the 33rd International Electric Propulsion Conference, The George Washington University, Washington, D.C., USA, October 6 - 10, 2013.

[24] I.M. Bronstein, B.S. Fraiman, eds., in "Vtorichnaya Elektronnaya Emissiya", (Nauka: Movkva), (1969) p. 340 (In Russian)